ACS Energy LETTERS

Cite This: ACS Energy Lett. 2019, 4, 1594−1601

http://pubs.acs.org/journal/aelccp

LETTER

Interfacial Sites between Cobalt Nitride and Cobalt Act as Bifunctional Catalysts for Hydrogen Electrochemistry

Fuzhan Song,[†,○] Wei Li,[†,○] Jiaqi Yang,[‡] Guanqun Han,[§] Tao Yan,[∥,⊥] Xi Liu,[#,▽] Yi Rao,[*,†] Peilin Liao,[*,‡] Zhi Cao,[*,∥,⊥,#] and Yujie Sun[*,†,§]

[†]Department of Chemistry & Biochemistry, Utah State University, Logan, Utah 84322, United States

[‡]School of Materials Engineering, Purdue University, West Lafayette, Indiana 47907, United States

[§]Department of Chemistry, University of Cincinnati, Cincinnati, Ohio 45221, United States

[∥]State Key Laboratory of Coal Conversion, Institute of Coal Chemistry, Chinese Academy of Sciences, Taiyuan 030001, China

[⊥]National Energy Center for Coal to Liquids, Synfuels CHINA Co., Ltd., Huairou District, Beijing 101400, China

[#]Syncat@Beijing, Synfuels China Technology Co., Ltd., Beijing 101407, China

[▽]School of Chemistry and Chemical Engineering, Shanghai Jiao Tong University, Shanghai 200240, China

Supporting Information

ABSTRACT: **Hydrogen (H_2) electrochemistry primarily consists of two reactions: hydrogen evolution reaction in water for H_2 production (HER) and hydrogen oxidation reaction in hydrogen fuel cells for H_2 utilization (HOR). The realization of future hydrogen economy necessitates the development of low-cost and competent electrocatalysts for both HER and HOR. Herein, we report that partial nitridation of cobalt nanoparticles on current collectors results in rich Co_2N/Co interfacial sites, which exhibit bifunctional activity for hydrogen electrochemistry, rivaling the state-of-the-art Pt counterparts tested under similar conditions. Our combined experimental and theoretical computation results demonstrate that Co_2N/Co interfacial sites not only possess optimal hydrogen adsorption energy but also facilitate water adsorption and dissociation on the catalyst surface, all of which are beneficial to the electrocatalytic performance for both HER and HOR. In addition, our Co_2N/Co electrocatalysts also demonstrate great tolerance against CO poisoning during long-term H_2 oxidation.**

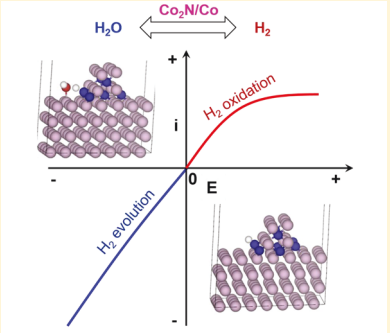

Interfacial Co_2N/Co sites active for both HER and HOR

Along with the increasing attention to exploring and utilizing sustainable energy sources, hydrogen (H_2) electrochemistry has attracted intense interest as H_2 production and oxidation play pivotal roles in the future hydrogen economy.[1,2] In order to be economically attractive, low-cost and competent electrocatalysts are indispensable for both H_2 evolution and oxidation reactions (HER and HOR).[3,4] Even though platinum-group metals, including Pt, Ir, Pd, and Rh, are still the state-of-the-art electrocatalysts of HER and HOR, their activities diminish quickly with along the increase of electrolyte pH.[5] Consequently, there is a rise of research interest in developing earth-abundant electrocatalysts for hydrogen electrochemistry under neutral and alkaline conditions.[6−8]

Because hydrogen adsorption energy (ΔG_{Had}) has been suggested as a common descriptor in predicting the activity of an electrocatalyst for HER and HOR, considerable efforts have been devoted to optimizing ΔG_{Had} through composition tuning,[9−11] alloying,[12] surface modification,[13−15] defect introduction,[16,17] and molecular design.[18,19] In neutral and alkaline electrolytes, water adsorption and dissociation have been recognized as critical steps in electrocatalytic H_2 evolution. Great success has been achieved in creating earth-abundant electrocatalysts for HER probably due to the enormous interest in water splitting during the past decade;[20−22] however, relatively less progress has been achieved in HOR,[23−26] even though HOR is a very important reaction for H_2 utilization in fuel cells. For example, a variety of metal nitride materials have been explored for electrocatalytic HER including Pt-decorated Ni_3N nanosheets,[27] Co/Ni_3N nanorods,[28] rodlike Co_xNi_yN,[29] $Co_{5.47}N$/N-doped carbon polyhedral,[30] graphdiyne-wrapped CoN_x nanosheets,[31] CoN/Ni_3N nanowires,[32] Co/CoN Janus nanoparticles embedded in N-doped carbon,[33] core−shell Co_2P-CoN nanoparticles in N-

Received: April 5, 2019
Accepted: June 12, 2019
Published: June 12, 2019

DOI: 10.1021/acsenergylett.9b00738
ACS Energy Lett. 2019, 4, 1594−1601

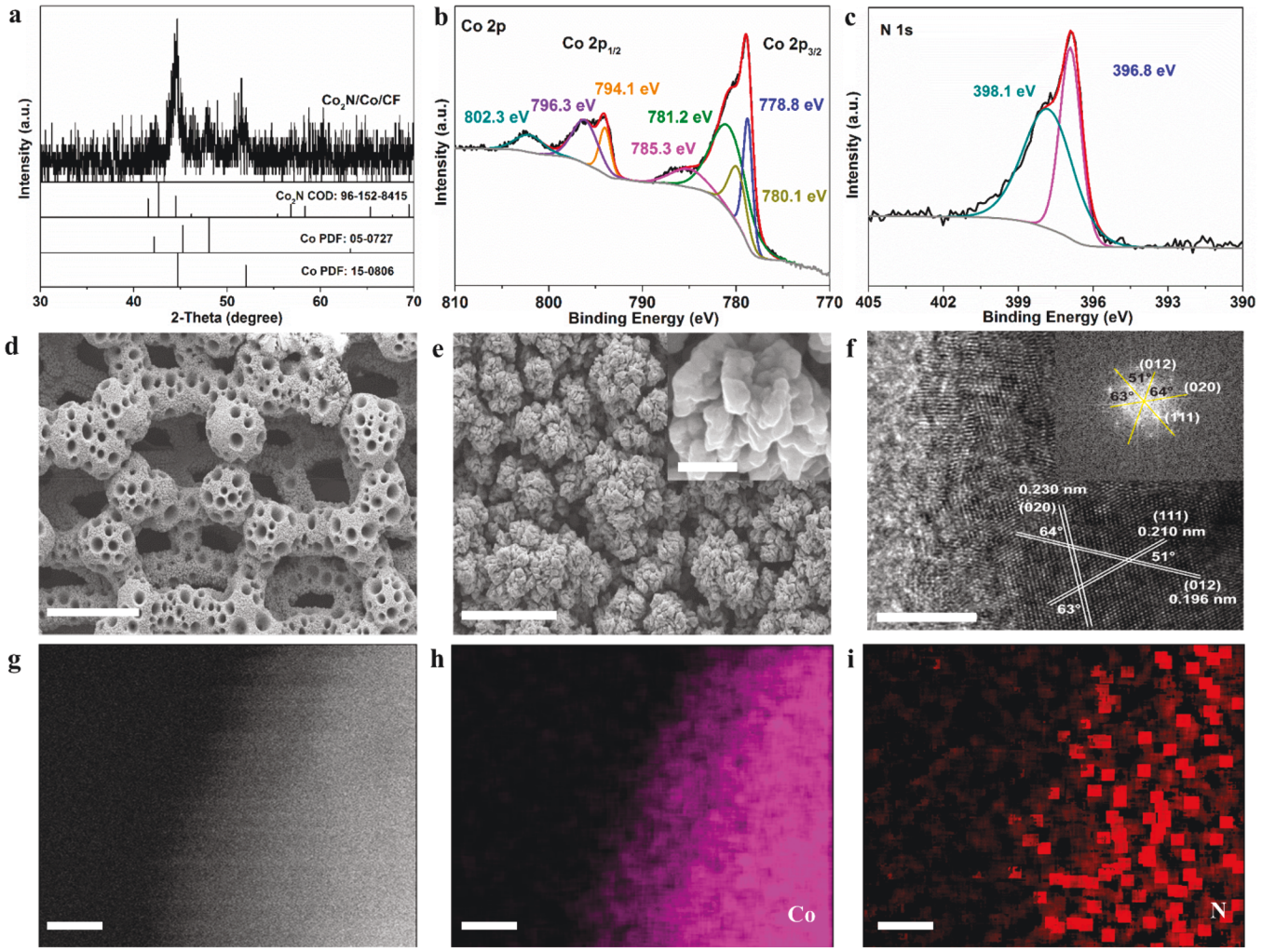

Figure 1. (a) XRD pattern of Co_2N/Co/CF and the standard XRD patterns of Co_2N and Co (cubic and hexagonal phases) as reference. (b,c) High-resolution Co 2p (b) and N 1s (c) XPS spectra of Co_2N/Co/CF. (d,e) SEM images of Co_2N/Co/CF at different magnifications. (f) HRTEM image showing the Co_2N component in Co_2N/Co/CF. The inset is a FFT pattern. (g–i) HAADF-STEM and corresponding elemental mapping images of Co and N in Co_2N/Co/CF. Scale bars: (d) 500 μm; (e) 10 μm (500 nm in the inset); (f) 5 nm; and (g–i) 2.5 nm.

doped carbon nanotubes,[34] and Co_4N nanowires on carbon cloth.[35] By creating heterostructures and tuning compositions, scientists have developed metal nitrides with much improved HER performance. However, most of the reported metal nitrides electrocatalysts require energy-intensive hydrothermal treatment, expensive metal organic framework (MOF) templates, and complex organic polymerization, impeding their large-scale production. Moreover, those reported metal nitride electrocatalysts still need relatively large overpotentials (68–190 mV) to deliver a HER benchmark current density of −10 mA cm^{-2} in neutral and alkaline electrolytes. Furthermore, the electrocatalytic HOR activity of metal nitrides has been barely investigated.[23−25]

Recently, we reported a bifunctional electrocatalyst of Ni_3N/Ni for both HER and HOR by creating interfacial sites between Ni_3N and Ni. Such an interfacing strategy shows great promise in developing competent hydrogen electrodes for water electrolyzers and hydrogen fuel cells.[36] However, it is unclear whether this strategy can be applied to construct other bifunctional transition metal-based electrocatalysts. Moreover, the relatively low hardness of nickel used in our previous work makes it difficult to be applied in producing structurally rigid electrodes,[37] and the substrate nickel foam may also complicate the elucidation of the real performance of the active sites in Ni_3N/Ni. Hence, it is desirable to explore reactive inert, structurally flexible, and also low-cost electrode substrates with alternative electrocatalyts containing metal/compound interfaces.

Herein, we extend our interfacing strategy to the preparation of a bifunctional cobalt-based electrocatalyst and report that the interfacial sites between cobalt nitride and cobalt nanoparticles formed on cobalt foam (Co_2N/Co/CF) or carbon paper (Co_2N/Co/CP) exhibit superior bifunctional activity for hydrogen electrochemistry, rivaling that of Pt-based electrocatalysts evaluated under similar conditions. Our electrodeposition and nitridation steps can be carried out under atmospheric pressure in a facile and scalable manner, which is beneficial to the large-scale production of electrocatalysts. To the best of our knowledge, the resultant interfacial Co_2N/Co electrocatalyst demonstrates extraordinary catalytic HER performance superior to that of nearly all reported cobalt-based electrocatalysts for both HER and HOR. Density functional theory (DFT) computational results support the fact that Co_2N/Co interfacial sites bear suitable hydrogen and

DOI: 10.1021/acsenergylett.9b00738
ACS Energy Lett. 2019, 4, 1594−1601

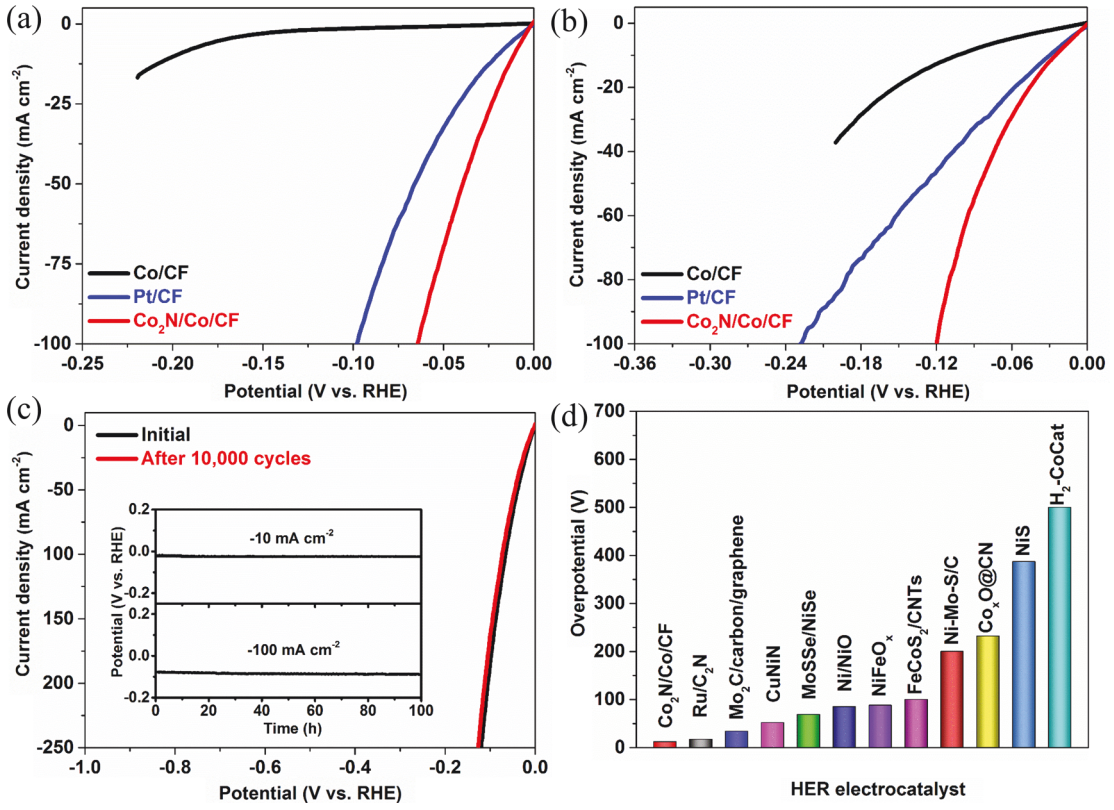

Figure 2. LSV curves of Co_2N/Co/CF, Pt/CF, and Co/CF for HER in 1.0 M KOH (a) and 1.0 M KPi (b). (c) LSV curves of Co_2N/Co/CF before and after 10 000 cycles at a scan rate of 100 mV s^{-1} between 0 and −100 mV vs RHE in 1.0 M KOH. The inset shows the chronopotentiometry curves of Co_2N/Co/CF conducted at −10 and −100 mA cm^{-2} without *iR* correction. (d) Comparison of overpotential requirements of selected HER electrocatalysts to deliver −10 mA cm^{-2} for HER in 1.0 M KOH. All LSV curves were *iR*-corrected.

water adsorption energies and also facilitate water dissociation, all of which are believed to contribute to the overall activity of Co_2N/Co toward HER and HOR. Another exciting observation is that Co_2N/Co shows great tolerance to CO poisoning, which is widely known of plaguing Pt during long-term H_2 oxidation. The success of Co_2N/Co demonstrates an effective strategy of interfacing metals and metal compounds (e.g., metal nitrides) for enhanced hydrogen electrochemistry.

The synthesis of Co_2N/Co/CF started from the electrodeposition of highly porous cobalt nanoparticles on cobalt foam (Co/CF) followed by thermal nitridation in ammonia (see details in the Supporting Information). The X-ray diffraction pattern of Co_2N/Co/CF obtained from nitridation at 350 °C for 3 h is shown in Figure 1a (other samples are shown in Figures S1 and S2), indicating the presence of orthorhombic Co_2N, hexagonal Co, and cubic Co phases despite the background noise caused by the fluorescence interference of Co. The valence states of surface composition elements in Co_2N/Co/CF were probed via X-ray photoelectron spectroscopy (XPS). Figure 1b shows the high-resolution Co 2p XPS spectrum. The peaks at 780.1 and 796.3 eV can be assigned to Co−N, which are consistent with reported cobalt nitride.[35,38] The broad peaks at 785.3 and 802.3 eV are satellite peaks. The peak at 781.2 eV is assigned to Co^{3+} due to surface oxidation upon exposure to air.[38] The peaks at 778.8 and 794.1 eV are ascribed to metallic Co $2p_{3/2}$ and $2p_{1/2}$, respectively,[39] which is in agreement with those of pristine Co (Figure S3a,b). The Co 2p XPS results indicate the presence of both metallic cobalt and cobalt nitride in Co_2N/Co/CF. For the N 1s region (Figure 1c), the main peak observed at 396.8 eV can be ascribed to the nitrogen species in Co_2N, while the shoulder peak at 398.1 eV likely results from the residual NH moieties of incomplete reaction with NH_3. The surface morphology of Co_2N/Co/CF was characterized by scanning electron microscopy (SEM) and compared to those of the parent Co/CF and pristine cobalt foam (CF). In contrast to the pristine CF with a smooth skeleton (Figure S4a,b), Co_2N/Co/CF displays a macroporous network structure of rough ligaments with numerous stacked particles over the skeleton surface (Figure 1d,e). Such a three-dimensional structure was mainly inherited from the parent Co/CF (Figure S4c,d). To further clearly identify the cobalt nitride phase among various polymorphs, a selected Co_2N crystal grain was characterized by high-resolution transmission electron microscopy (HRTEM). The well-resolved lattice fringes (Figure 1f) with interplanar spacing of 0.230, 0.210, and 0.196 nm measured through fast Fourier transform (FFT) correspond to the crystal planes of (020), (111), and (012) of Co_2N, respectively. The intersection angles between the two planes match very well with the theoretical values, which is direct evidence for the formation of orthorhombic Co_2N and also consistent with the XRD results.[40] To identify the Co_2N/Co interfacial sites, a HRTEM image of the Co_2N/Co interfacial region in Co_2N/Co/CF was collected and is shown in Figure S5a. Two kinds of spots in FFT of the selected area can be identified; one set includes larger spots, and another set has smaller dots (Figure S5b). The IFFT image from the selected larger sports (Figure S5c,d) indicates very crystalline metallic cobalt with its [111] zone-axis along the electron beam direction. However, the IFFT image from

DOI: 10.1021/acsenergylett.9b00738
ACS Energy Lett. 2019, 4, 1594−1601

the selected smaller dots (Figure S5e,f) clearly shows the formation of small Co_2N nanoparticles in a cobalt matrix with te zone-axis along [1−10]. In addition, scanning transmission electron microscopy (STEM) combined with energy-dispersive X-ray (EDX) mapping results obtained from the identical area is shown in Figures 1g−i and S6. Apparently, the nitrogen distribution in the composite is not uniform at the nanoscale, which indicates the presence of small nitride nanoparticles on the cobalt surface. EDX spectra from the selected areas (Figure S7) also show significantly different nitrogen contents in the different areas, even at the nanoscale. Collectively, these characterization results validate the formation of Co_2N on Co/CF, as well as Co_2N/Co interfacial sites in Co_2N/Co/CF.

Co_2N/Co/CF was first evaluated for its electrocatalytic H_2 evolution activity in both H_2-saturated alkaline (1.0 M KOH) and neutral (1.0 M potassium phosphate, KPi) electrolytes. All potentials reported herein are referenced to the reversible hydrogen electrode (RHE), and the reported current densities were normalized based on the geometric area of the electrode for the comparison of apparent activity. It should be noted that both nitridation temperature and duration were varied to achieve the optimized electrocatalyst, and it was found that nitridation at 350 °C for 3 h yielded a Co_2N/Co/CF sample with the best HER performance at both pH 7 and 14 (Figures S8−S11). Therefore, the Co_2N/Co/CF samples discussed in the following paragraphs were synthesized according to this optimized condition unless noted otherwise. For comparison, the pristine Co/CF and commercial Pt/C (20%) loaded on bare CF (Pt/CF) were also tested for catalytic HER under the same conditions. The loading mass of Pt/C was varied to achieve the best HER performance in both alkaline and neutral electrolytes (Figures S12 and S13). Figure 2a,b plots the linear sweep voltammetry (LSV) curves of Co_2N/Co/CF, Pt/CF, and Co/CF in 1.0 M KOH and KPi, respectively. In both alkaline and neutral electrolytes, Co_2N/Co/CF exhibited a catalytic HER takeoff at near-zero overpotential, similar to the benchmark Pt/CF. However, Co/CF required a much larger overpotential to initiate H_2 evolution. In 1.0 M KOH (Figure 2a), Co_2N/Co/CF was able to produce −10 and −100 mA/cm^2 at overpotential of merely 12 and 64 mV, respectively, substantially smaller than those required by Pt/CF (20 and 98 mV). At pH 7 (Figure 2b), Co_2N/Co/CF also exhibited excellent HER performance, demanding only 26 and 120 mV overpotentials to reach −10 and −100 mV/cm^2, which were apparently superior to Pt/CF tested under the same condition. The Tafel plots of Co_2N/Co/CF derived from their LSVs are shown in Figures S14 and S15. The Tafel slopes of Co_2N/Co/CF for HER in 1.0 M KOH and 1.0 M KPi were as low as 41.6 and 87.5 mV/decade, respectively, which are even smaller than those of Pt (73.3 and 108.5 mV/decade). These Tafel slopes of Co_2N/Co/CF indicate that the electrocatalytic HER kinetics likely follows the Heyrovsky mechanism ($H_2O + M{-}H^* + e^- = M + H_2 + OH^-$), where H* represents a hydrogen atom absorbed on a catalyst surface. The rate-limiting step of HER on Co_2N/Co/CF is closely related to the initial water dissociation and the subsequent H* adsorption.

The aforementioned HER performance based on the apparent current density could be overestimated for an electrocatalyst because of its highly porous structure. In order to make a fair comparison between Co_2N/Co/CF and the state-of-the-art Pt in electrocatalytic H_2 evolution, we further measured their respective electrochemically active surface area (ESCA) and normalized the obtained current against the corresponding ECSA of each catalyst. It should be noted that all of the ECSA measurements were conducted in anhydrous acetonitrile with the aim of excluding the impact of hydration and protonation commonly observed for first-row transition metal compounds in aqueous media.[41] Although the ECSA of Co_2N/Co/CF is 2.38 times lower than that of Pt/CF (2.5 mg cm^{-2}) (Figure S16a−d), the ECSA-normalized current densities of Co_2N/Co/CF for HER are still much higher than those of Pt/CF in both alkaline and neutral electrolytes (Figures S17 and S18). Figures S19a,b and S20a,b show the Nyquist plots with fitting curves and an equivalent circuit model and the Bode plots of Co_2N/Co/CF and Co/CF for HER at given potentials in 1.0 M KOH and KPi. The fitting results are listed in Table S1, showing the much smaller charge transfer resistance and fast kinetics of HER on Co_2N/Co/CF than those on Co/CF in both basic and neutral electrolytes.

To demonstrate that the excellent HER performance of Co_2N/Co is independent of the underlying current collector, such as the cobalt foam, we further synthesized Co_2N/Co on carbon paper (Co_2N/Co/CP) following the same synthetic procedure of Co_2N/Co/CF except for replacing CF with carbon paper. A suite of characterizations (XRD, SEM, and XPS) were also conducted on Co_2N/Co/CP (Figures S21, S22a,b, and S23a−d) to confirm the presence of Co_2N/Co with similar composition and morphology as those of Co_2N/Co/CF. Figure S24 presents the LSV and chronopotentiometry curves of Co_2N/Co/CP compared to those of Co_2N/Co/CF. The near overlap of these curves proves that the great HER performance of Co_2N/Co does not rely on a particular current collector; instead, it most likely originates from the real active sites located on Co_2N/Co.

Besides intrinsic activity, long-term stability is another important criterion in assessing any catalysts. The robustness of Co_2N/Co/CF for extended H_2 evolution was evaluated via repetitive cyclic voltammetry (CV) and chronopotentiometry. As depicted in Figure 2c, after 10 000 CV cycles, the HER overpotential of Co_2N/Co/CF required to achieve −100 mA cm^{-2} only increased by 7 mV in 1.0 M KOH. In addition, the stable chronopotentiometry curves collected at −10 and −100 mA/cm^2 for 100 h (Figure 2c inset) further corroborated its great robustness for long-term H_2 evolution. Similar stability was observed for Co_2N/Co/CF in neutral electrolyte (Figures S25 and S26). Postelectrolysis characterization revealed no apparent change in the morphology and composition of Co_2N/Co/CF (Figure S27a−d), implying its outstanding structural robustness and mechanical stability. Furthermore, the produced H_2 amount matched well the theoretically calculated quantity (Figure S28), which indicated that all of the passed charge was used to generate H_2, resulting in a nearly 100% Faradaic efficiency. Overall, to the best of our knowledge, Co_2N/Co/CF represents one of the most active HER electrocatalysts in alkaline and neutral electrolytes, surpassing a great number of reported nonprecious electrocatalysts (Figure 2d and Table S2).

Next, DFT computation was carried out to aid the understanding of the superior activity of Co_2N/Co/CF for H_2 production. We reasoned that a suitable model structure of Co_2N/Co is a few layers of Co_2N positioned on a Co basal plane. For a systematic comparison, three model systems with the lowest-energy surfaces of Co_2N(001), Co(001), and hybrid Co_2N/Co with a Co_2N(001) slab in contact with the Co(001) surface were considered. Due to the lack of free H^+ in neutral and alkaline electrolytes, the commencement of electrocatalytic

DOI: 10.1021/acsenergylett.9b00738
ACS Energy Lett. 2019, 4, 1594−1601

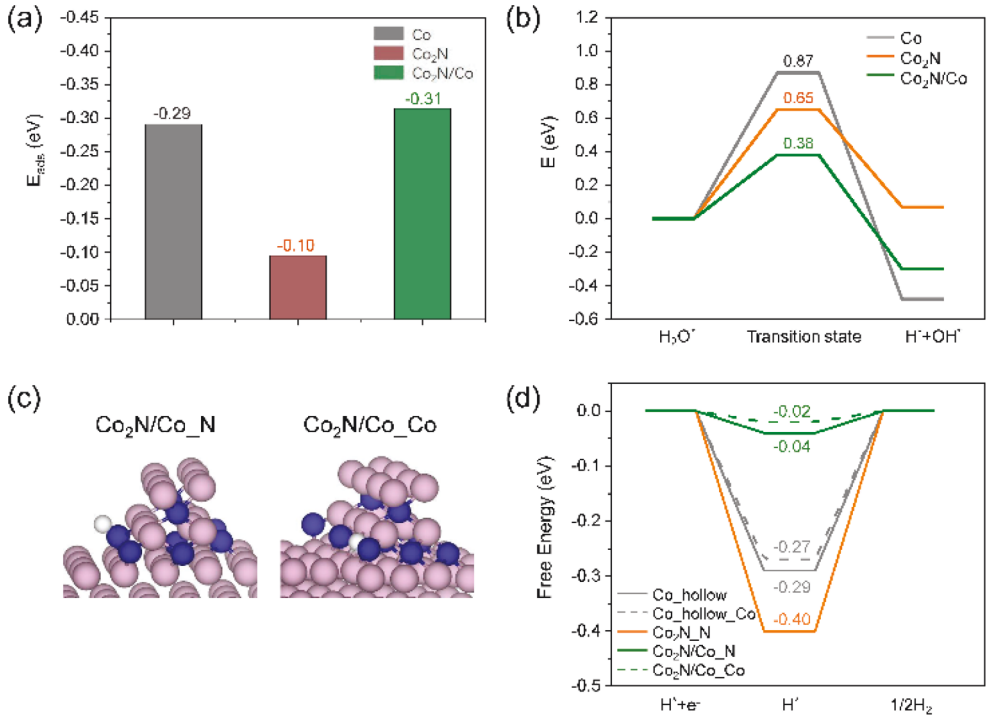

Figure 3. (a) Water adsorption energy on Co, Co_2N, and Co_2N/Co. (b) Reaction energetics for water dissociation on Co, Co_2N, and Co_2N/Co. (c) Optimized structures of H adsorption at two different positions of interfacial Co_2N/Co. Color code: pink (Co), blue (N), and white (H). (d) Free energy changes (ΔG_{Had}) of H adsorption on Co, Co_2N, and Co_2N/Co.

H_2 evolution at pH 7 and 14 demands water adsorption and dissociation on catalyst surface as the initial steps.[42] The computed water adsorption energies on Co_2N/Co, Co_2N, and Co are compared in Figure 3a with their respective adsorption configurations shown in Figures S29a,b, S30a,b, and S31a,b, respectively. It is apparent that Co_2N/Co exhibits the strongest water adsorption among the three models, and the optimal water adsorption site is located at the interface between Co_2N and Co in Co_2N/Co with one of the H atoms in water approaching the edge N in Co_2N (Figure S32a,b), probably due to the hydrogen bond interaction. Such a configuration of water adsorption on Co_2N/Co is believed to be beneficial for its subsequent dissociation. Indeed, as shown in Figure 3b, the critical transition state of water dissociation has the lowest energy on Co_2N/Co. The detailed structure and energy of each state for water dissociation on Co_2N/Co, Co_2N, and Co can be found in the Supporting Information (Figures S32a,b S33a,b, S34a,b, and S35a,b). A widely accepted consensus in hydrogen electrochemistry is that hydrogen adsorption free energy (ΔG_{Had}) on an electrocatalyst is a key descriptor of it activity.[43] A high catalytic performance is anticipated if ΔG_{Had} is close to 0 eV. Therefore, hydrogen adsorption on Co_2N/Co, Co_2N, and Co was also investigated computationally. The most plausible hydrogen adsorption sites on these models were considered (Figures S35−S44 and Table S3). The free energy changes of hydrogen adsorption at two interfacial sites of Co_2N/Co were calculated to be merely −0.02 and −0.04 eV, very close to the ideal value of 0 eV (Figure 3c,d). In contrast, both Co_2N and Co exhibit strong hydrogen affinity (−0.27 to −0.40 eV). Collectively, these DFT computational results demonstrate that the interfacial sites of Co_2N/Co can enhance water adsorption, facilitate water dissociation, and also exhibit optimal hydrogen adsorption energy, all of which contribute to its extraordinary HER activity.

Encouraged by the extremely small ΔG_{Had} value and nearly zero HER onset potential, we reasoned that Co_2N/Co could be a promising electrocatalyst for the reserve reaction of HER, the hydrogen oxidation reaction (HOR), as both HER and HOR share the same critical intermediate, adsorbed H (H_{ad}).[4,44] The HOR performance of Co_2N/Co/CF was measured in H_2-saturated 0.1 M KOH electrolyte to mimic the alkaline condition of hydroxide exchange membrane fuel cells. Similar to HER, the best HOR activity was also obtained from Co_2N/Co/CF after nitridation at 350 °C for 3 h (Figures S45 and S46). Figure S47 compares the steady-state polarization curves of Co_2N/Co/CF collected in H_2- or Ar-saturated 0.1 M KOH in the same potential region of −0.06−0.1 V vs RHE. The apparent anodic current at positive potential (vs RHE) was obtained only in the presence of H_2, suggesting that H_2 oxidation takes place on Co_2N/Co/CF. Commercial Pt/C with optimized loading (1.5 mg cm^{-2}) on CF (Pt/CF) was also included for comparison (Figure S48). As plotted in Figure 4a, the electrocatalytic HOR performance follows the order of Co_2N/Co/CF > Pt/CF > Co/CF. Co_2N/Co/CF showed a catalytic takeoff at 0 V vs RHE for HOR and produced higher current density than Pt/CF in the entire potential window (0−0.1 V vs RHE), even if the current density was normalized by their corresponding ECSA (Figure S49). In contrast, Co/CF displayed negligible catalytic activity for HOR, confirming that the enhanced HOR activity of Co_2N/Co/CF arises from the Co_2N/Co interfacial sites. In order to assess the intrinsic activity, the exchange current density was estimated from the micropolarization window from −10 to 10 mV vs RHE. Co_2N/Co/CF produced an exchange current density of −2.86 mA cm^{-2}, which was 1.4 and 28.5 times higher than that of Pt/CF and Co/CF, respectively (Figure S50). The stability of Co_2N/Co/CF for H_2 oxidation was further assessed by chronoamperometry at

DOI: 10.1021/acsenergylett.9b00738
ACS Energy Lett. 2019, 4, 1594−1601

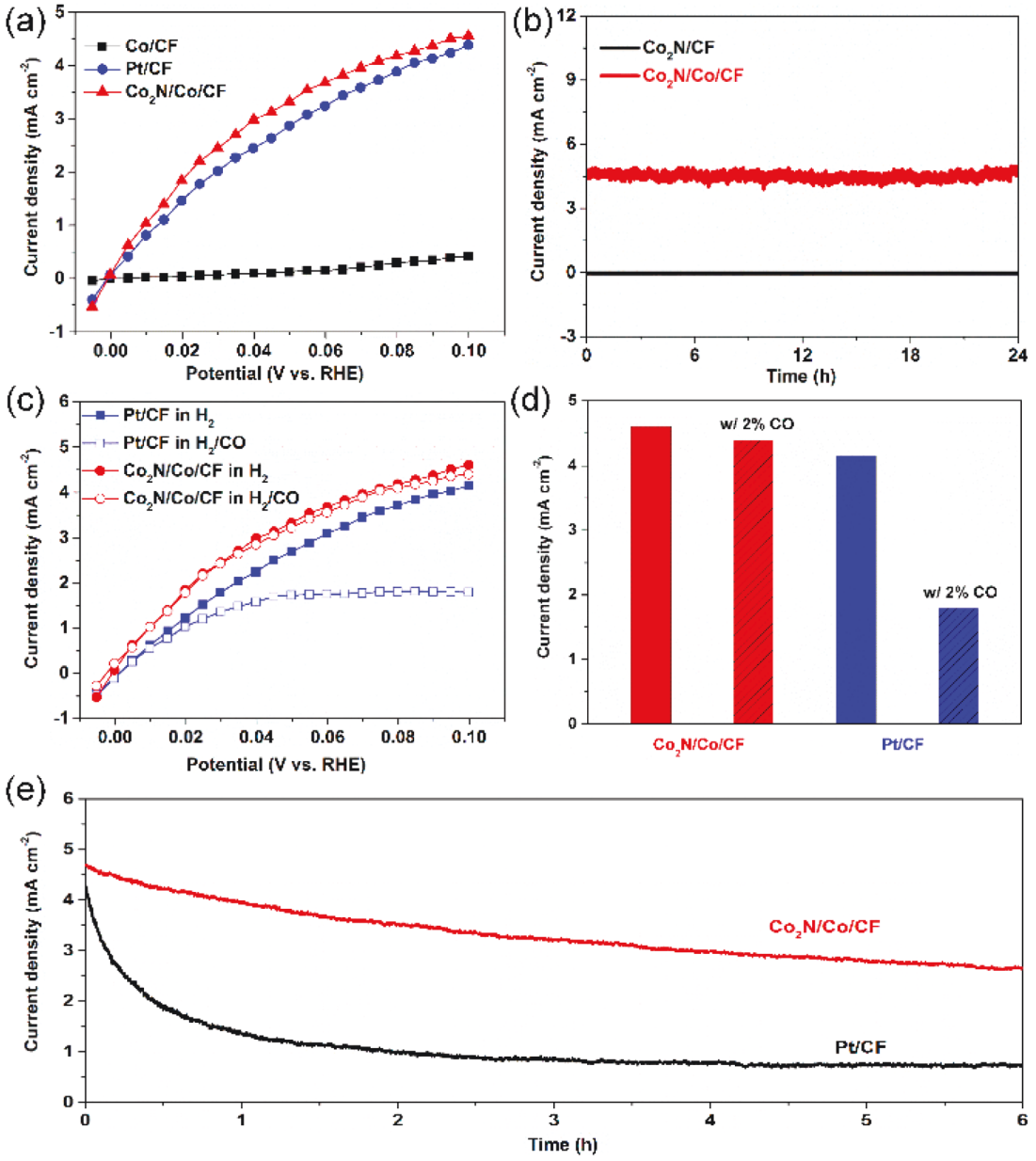

Figure 4. (a) Steady-state polarization curves of Co_2N/Co/CF, Co/CF, and Pt/CF for HOR in H_2-saturated 0.1 M KOH. (b) Chronoamperometry curves of Co_2N/Co/CF and Co/CF in H_2-saturated 0.1 M KOH measured at 0.09 V vs RHE. (c) Steady-state polarization curves and (d) comparison of the HOR performance of Co_2N/Co/CF and Pt/CF in 0.1 M KOH saturated with H_2 or H_2 with 2% (v/v) CO at 0.09 V vs RHE. (e) Chronoamperometry curves of Co_2N/Co/CF and Pt/CF in 0.1 M KOH saturated with H_2 with 2% (v/v) CO measured at 0.09 V vs RHE.

0.09 V vs RHE in 0.1 M KOH (Figure 4b), showing a stable current density of 4.5 mA cm^{-2} in the presence of H_2, in striking contrast to the negligible capacitance current density obtained in the Ar-saturated KOH (Figure S51). Without nitridation, Co/CF only delivered no more than 0.1 mA cm^{-2} in H_2-saturated 0.1 M KOH, in agreement with the crucial role of Co_2N/Co in catalyzing H_2 oxidation (Figure 4b). The excellent stability of Co_2N/Co/CF for H_2 oxidation was attributed to the robustness of Co_2N. Figures S52 and S53 present the XRD pattern and HRTEM image of Co_2N/Co/CF post HOR electrolysis, and the results indicate good retention of composition and retention of Co_2N/Co/CF after long-term electrolysis for H_2 oxidation in 0.1 M KOH. The XPS spectra of the postcatalysis Co_2N/Co/CF also exhibited little changes compared to that of pristine Co_2N/Co/CF (Figure S54).

Current industrial H_2 supply is mainly from steam reforming, producing cost-effective H_2 feeds yet with CO impurity, which is detrimental to Pt-based electrocatalysts.[45] Therefore, a high CO tolerance is desirable for HOR electrocatalysts. Herein, a CO tolerance test was also carried out for Co_2N/Co/CF and Pt/CF using a H_2 gas mixture with 2% CO (v/v). As shown in Figure 4c, the steady-state polarization curve of Co_2N/Co/CF showed no apparent degradation in the presence of CO, while Pt/CF indeed suffered from substantial CO poisoning. For instance, the anodic current density of Co_2N/Co/CF slightly decreased from 4.6 to 4.4 mA cm^{-2} at 0.09 V vs RHE upon the addition of 2% CO in the H_2 feed (Figure 4d), whereas the current density of Pt/CF was dramatically reduced by 57%, decreasing from 4.15 to 1.79 mA cm^{-2}. Co_2N/Co/CF also exhibited a

DOI: 10.1021/acsenergylett.9b00738
ACS Energy Lett. 2019, 4, 1594−1601

much longer robustness than Pt/CF toward CO poisoning (Figure 4e). The anodic current density of Co_2N/Co/CF remained at ca. 3.5 mA cm^{-2} after 6 h when electrolysis at 0.09 V vs RHE was carried out with a feed of 2% CO in H_2, whereas a current density of only 0.7 mA cm^{-2} was produced on Pt/CF under the same condition.

In summary, we successfully constructed low-cost Co_2N/Co electrocatalysts through a facile electrodeposition and nitridation approach. The interfacial sites of Co_2N/Co exhibit excellent performance for both H_2 evolution and oxidation reactions, rivaling the activity of Pt-based electrocatalysts evaluated under similar conditions. Together with its remarkable CO tolerance, Co_2N/Co is a great catalyst candidate in the applications of water electrolyzers and alkaline hydrogen fuel cells. DFT calculations revealed the critical role of Co_2N/Co interfacial sites in promoting the adsorption and dissociation of water and optimizing the free energy of hydrogen adsorption. This work showcases that interface construction between metals and metal nitrides is an effective strategy in developing competent catalysts for the hydrogen electrochemistry.

■ ASSOCIATED CONTENT

Supporting Information

The Supporting Information is available free of charge on the ACS Publications website at DOI: 10.1021/acsenergylett.9b00738.

Details of the experimental methods, instruments, SEM, XRD, XPS, STEM-EDX, HRTEM, and electrochemical measurements (PDF)

■ AUTHOR INFORMATION

Corresponding Authors

*E-mail: yujie.sun@usu.edu.
*E-mail: caozhi@sxicc.ac.cn.
*E-mail: lpl@purdue.edu.
*E-mail: yi.rao@usu.edu.

ORCID

Yi Rao: 0000-0001-9882-1314
Yujie Sun: 0000-0002-4122-6255

Author Contributions

○F.S. and W.L. contributed equally to this work.

Notes

The authors declare no competing financial interest.

■ ACKNOWLEDGMENTS

We acknowledge financial support of the UTAG program of USTAR, State of Utah. Y.S. acknowledges the financial support of the Herman Frasch Foundation (820-HF17), the National Science Foundation (CHE-1653978, CHE-1914546), Utah State University (USU), and University of Cincinnati. We acknowledge the Microscopy Core Facility at USU. P.L. thanks the ACS Petroleum Research Foundation for the support of this research. The computational research was supported in part through computational resources provided by the Information Technology department at Purdue University. Z.C. is grateful for the financial support from Synfuels China, Co. Ltd. Z.C. also acknowledges the innovation foundation of the Institute of Coal Chemistry, Chinese Academy of Sciences, Hundred-Talent Program of Chinese Academy of Sciences, and Shanxi Hundred-Talent Program.

■ REFERENCES

(1) Stamenkovic, V. R.; Strmcnik, D.; Lopes, P. P.; Markovic, N. M. Energy and fuels from electrochemical interfaces. *Nat. Mater.* **2017**, *16*, 57−69.

(2) Setzler, B. P.; Zhuang, Z.; Wittkopf, J. A.; Yan, Y. Activity targets for nanostructured platinum-group-metal-free catalysts in hydroxide exchange membrane fuel cells. *Nat. Nanotechnol.* **2016**, *11*, 1020−1025.

(3) Cong, Y.; Yi, B.; Song, Y. Hydrogen oxidation reaction in alkaline media: From mechanism to recent electrocatalysts. *Nano Energy* **2018**, *44*, 288−303.

(4) Sheng, W.; Zhuang, Z.; Gao, M.; Zheng, J.; Chen, J. G.; Yan, Y. Correlating hydrogen oxidation and evolution activity on platinum at different pH with measured hydrogen binding energy. *Nat. Commun.* **2015**, *6*, 5848.

(5) Durst, J.; Siebel, A.; Simon, C.; Hasché, F.; Herranz, J.; Gasteiger, H. A. New insights into the electrochemical hydrogen oxidation and evolution reaction mechanism. *Energy Environ. Sci.* **2014**, *7*, 2255−2260.

(6) Song, F.; Li, W.; Han, G.; Sun, Y. Electropolymerization of aniline on nickel-based electrocatalysts substantially enhances their performance for hydrogen evolution. *ACS Appl. Energy Mater.* **2018**, *1*, 3−8.

(7) Li, W.; Jiang, N.; Hu, B.; Liu, X.; Song, F.; Han, G.; Jordan, T. J.; Hanson, T. B.; Liu, T. L.; Sun, Y. Electrolyzer design for flexible decoupled water splitting and organic upgrading with electron reservoirs. *Chem.* **2018**, *4*, 637−649.

(8) You, B.; Liu, X.; Hu, G.; Gul, S.; Yano, J.; Jiang, D.-e.; Sun, Y. Universal surface engineering of transition metals for superior electrocatalytic hydrogen evolution in neutral water. *J. Am. Chem. Soc.* **2017**, *139*, 12283−12290.

(9) Subbaraman, R.; Tripkovic, D.; Strmcnik, D.; Chang, K.-C.; Uchimura, M.; Paulikas, A. P.; Stamenkovic, V.; Markovic, N. M. Enhancing hydrogen evolution activity in water splitting by tailoring Li^+-Ni $(OH)_2$-Pt interfaces. *Science* **2011**, *334*, 1256−1260.

(10) Jiang, N.; You, B.; Sheng, M.; Sun, Y. Electrodeposited cobalt-phosphorous-derived films as competent bifunctional catalysts for overall water splitting. *Angew. Chem., Int. Ed.* **2015**, *54*, 6251−6254.

(11) Xu, J.; Liu, T.; Li, J.; Li, B.; Liu, Y.; Zhang, B.; Xiong, D.; Amorim, I.; Li, W.; Liu, L. Boosting the hydrogen evolution performance of ruthenium clusters through synergistic coupling with cobalt phosphide. *Energy Environ. Sci.* **2018**, *11*, 1819−1827.

(12) Lv, H.; Xi, Z.; Chen, Z.; Guo, S.; Yu, Y.; Zhu, W.; Li, Q.; Zhang, X.; Pan, M.; Lu, G.; Mu, S.; Sun, S. A new core/shell NiAu/Au nanoparticle catalyst with Pt-like activity for hydrogen evolution reaction. *J. Am. Chem. Soc.* **2015**, *137*, 5859−5862.

(13) Yang, Y.; Luo, M.; Zhang, W.; Sun, Y.; Chen, X.; Guo, S. Metal surface and interface energy electrocatalysis: fundamentals, performance engineering, and opportunities. *Chem.* **2018**, *4*, 2054−2083.

(14) Seh, Z. W.; Kibsgaard, J.; Dickens, C. F.; Chorkendorff, I.; Nørskov, J. K.; Jaramillo, T. F. Combining theory and experiment in electrocatalysis: insights into materials design. *Science* **2017**, *355*, eaad4998.

(15) Zeng, Z.; Chang, K.-C.; Kubal, J.; Markovic, N. M.; Greeley, J. Stabilization of ultrathin (hydroxy) oxide films on transition metal substrates for electrochemical energy conversion. *Nat. Energy* **2017**, *2*, 17070.

(16) Xie, J.; Zhang, H.; Li, S.; Wang, R.; Sun, X.; Zhou, M.; Zhou, J.; Lou, X. W.; Xie, Y. Defect-rich MoS_2 ultrathin nanosheets with additional active edge sites for enhanced electrocatalytic hydrogen evolution. *Adv. Mater.* **2013**, *25*, 5807−5813.

(17) Fan, X.; Liu, Y.; Chen, S.; Shi, J.; Wang, J.; Fan, A.; Zan, W.; Li, S.; Goddard, W. A.; Zhang, X.-M. Defect-enriched iron fluoride-oxide nanoporous thin films bifunctional catalyst for water splitting. *Nat. Commun.* **2018**, *9*, 1809.

(18) Thoi, V. S.; Sun, Y.; Long, J. R.; Chang, C. J. Complexes of earth-abundant metals for catalytic electrochemical hydrogen generation under aqueous conditions. *Chem. Soc. Rev.* **2013**, *42*, 2388−2400.

DOI: 10.1021/acsenergylett.9b00738
ACS Energy Lett. 2019, 4, 1594−1601

(19) Raugei, S.; DuBois, D. L.; Rousseau, R.; Chen, S.; Ho, M.-H.; Bullock, R. M.; Dupuis, M. Toward molecular catalysts by computer. *Acc. Chem. Res.* **2015**, *48*, 248−255.
(20) Kanan, M. W.; Nocera, D. G. In situ formation of an oxygen-evolving catalyst in neutral water containing phosphate and Co^{2+}. *Science* **2008**, *321*, 1072−1075.
(21) Nocera, D. G. Solar fuels and solar chemicals industry. *Acc. Chem. Res.* **2017**, *50*, 616−619.
(22) You, B.; Sun, Y. Innovative strategies for electrocatalytic water splitting. *Acc. Chem. Res.* **2018**, *51*, 1571−1580.
(23) Sheng, W.; Bivens, A. P.; Myint, M.; Zhuang, Z.; Forest, R. V.; Fang, Q.; Chen, J. G.; Yan, Y. Non-precious metal electrocatalysts with high activity for hydrogen oxidation reaction in alkaline electrolytes. *Energy Environ. Sci.* **2014**, *7*, 1719−1724.
(24) Zhuang, Z.; Giles, S. A.; Zheng, J.; Jenness, G. R.; Caratzoulas, S.; Vlachos, D. G.; Yan, Y. Nickel supported on nitrogen-doped carbon nanotubes as hydrogen oxidation reaction catalyst in alkaline electrolyte. *Nat. Commun.* **2016**, *7*, 10141.
(25) Gao, L.; Wang, Y.; Li, H.; Li, Q.; Ta, N.; Zhuang, L.; Fu, Q.; Bao, X. A nickel nanocatalyst within a h-BN shell for enhanced hydrogen oxidation reactions. *Chem. Sci.* **2017**, *8*, 5728−5734.
(26) Kabir, S.; Lemire, K.; Artyushkova, K.; Roy, A.; Odgaard, M.; Schlueter, D.; Oshchepkov, A.; Bonnefont, A.; Savinova, E.; Sabarirajan, D. C.; Mandal, P.; Crumlin, E. J.; Zenyuk, I.; Atanassov, P.; Serov, A. Platinum group metal-free NiMo hydrogen oxidation catalysts: high performance and durability in alkaline exchange membrane fuel cells. *J. Mater. Chem. A* **2017**, *5* (46), 24433−24443.
(27) Wang, Y.; Chen, L.; Yu, X.; Wang, Y.; Zheng, G. Superb alkaline hydrogen evolution and simultaneous electricity generation by Pt-decorated Ni_3N Nanosheets. *Adv. Energy Mater.* **2017**, *7*, 1601390.
(28) Zhu, C.; Wang, A.-L.; Xiao, W.; Chao, D.; Zhang, X.; Tiep, N.; Chen, S.; Kang, J.; Wang, X.; Ding, J.; Wang, J.; Zhang, H.; Fan, H. J. In situ grown epitaxial heterojunction exhibits high-performance electrocatalytic water splitting. *Adv. Mater.* **2018**, *30*, 1705516.
(29) Feng, X.; Wang, H.; Bo, X.; Guo, L. Bimetal-organic framework-derived porous rodlike cobalt/nickel nitride for all-pH value electrochemical hydrogen evolution. *ACS Appl. Mater. Interfaces* **2019**, *11*, 8018−8024.
(30) Chen, Z.; Ha, Y.; Liu, Y.; Wang, H.; Yang, H.; Xu, H.; Li, Y.; Wu, R. In situ formation of cobalt nitrides/graphitic carbon composites as efficient bifunctional electrocatalysts for overall water splitting. *ACS Appl. Mater. Interfaces* **2018**, *10*, 7134−7144.
(31) Fang, Y.; Xue, Y.; Hui, L.; Yu, H.; Liu, Y.; Xing, C.; Lu, F.; He, F.; Liu, H.; Li, Y. In situ growth of graphdiyne based heterostructure: toward efficient overall water splitting. *Nano Energy* **2019**, *59*, 591−597.
(32) Ray, C.; Lee, S. C.; Jin, B.; Kundu, A.; Park, J. H.; Jun, S. C. Conceptual design of three-dimensional CoN/Ni_3N-coupled nanograsses integrated on N-doped carbon to serve as efficient and robust water splitting electrocatalysts. *J. Mater. Chem. A* **2018**, *6*, 4466−4476.
(33) Fan, M.; Zheng, Y.; Li, A.; Li, K.; Liu, H.; Qiao, Z. Janus CoN/Co cocatalyst in porous N-doped carbon: toward enhanced catalytic activity for hydrogen evolution. *Catal. Sci. Technol.* **2018**, *8*, 3695−3703.
(34) Guo, Y.; Yuan, P.; Zhang, J.; Xia, H.; Cheng, F.; Zhou, M.; Li, J.; Qiao, Y.; Mu, S.; Xu, Q. Co_2P-CoN double active centers confined in N-doped carbon nanotube: heterostructural engineering for trifunctional catalysis toward HER, ORR, OER, and Zn-air batteries driven water splitting. *Adv. Funct. Mater.* **2018**, *28*, 1805641.
(35) Xue, Z.; Kang, J.; Guo, D.; Zhu, C.; Li, C.; Zhang, X.; Chen, Y. Self-supported cobalt nitride porous nanowire arrays as bifunctional electrocatalyst for overall water splitting. *Electrochim. Acta* **2018**, *273*, 229−238.
(36) Song, F.; Li, W.; Yang, J.; Han, G.; Liao, P.; Sun, Y. Interfacing nickel nitride and nickel boosts both electrocatalytic hydrogen evolution and oxidation reactions. *Nat. Commun.* **2018**, *9*, 4531.
(37) Samsonov, G. V. Mechanical properties of the elements. *Handbook of the physicochemical properties of the elements*; 1968; pp 387−446.
(38) Liu, C.; Bai, G.; Tong, X.; Wang, Y.; Lv, B.; Yang, N.; Guo, X. Mesoporous and ultrathin arrays of cobalt nitride nanosheets for electrocatalytic oxygen evolution. *Electrochem. Commun.* **2019**, *98*, 87−91.
(39) Lai, J.; Huang, B.; Chao, Y.; Chen, X.; Guo, S. Strongly coupled nickel-cobalt nitrides/carbon hybrid nanocages with Pt-like activity for hydrogen evolution catalysis. *Adv. Mater.* **2019**, *31*, 1805541.
(40) Clarke, J.; Jack, K. H. The preparation and the crystal structures of cobalt nitride, Co_2N, of cobalt carbonitrides, $Co_2(C, N)$, and of cobalt carbide, Co_2C. *Chem. Ind. (London)* **1951**, *46*, 1004−1005.
(41) Yoon, Y.; Yan, B.; Surendranath, Y. Suppressing ion transfer enables versatile measurements of electrochemical surface area for intrinsic activity comparisons. *J. Am. Chem. Soc.* **2018**, *140*, 2397−2400.
(42) Zhang, J.; Wang, T.; Liu, P.; Liao, Z.; Liu, S.; Zhuang, X.; Chen, M.; Zschech, E.; Feng, X. Efficient hydrogen production on $MoNi_4$ electrocatalysts with fast water dissociation kinetics. *Nat. Commun.* **2017**, *8*, 15437.
(43) Nørskov, J. K.; Bligaard, T.; Logadottir, A.; Kitchin, J. R.; Chen, J. G.; Pandelov, S.; Stimming, U. Trends in the exchange current for hydrogen evolution. *J. Electrochem. Soc.* **2005**, *152*, J23−J26.
(44) Zheng, J.; Sheng, W.; Zhuang, Z.; Xu, B.; Yan, Y. Universal dependence of hydrogen oxidation and evolution reaction activity of platinum-group metals on pH and hydrogen binding energy. *Sci. Adv.* **2016**, *2*, No. e1501602.
(45) Whittaker, T.; Kumar, K. B. S.; Peterson, C.; Pollock, M. N.; Grabow, L. C.; Chandler, B. D. H_2 oxidation over supported Au nanoparticle catalysts: evidence for heterolytic H_2 activation at the metal-support interface. *J. Am. Chem. Soc.* **2018**, *140*, 16469−16487.

DOI: 10.1021/acsenergylett.9b00738
ACS Energy Lett. 2019, 4, 1594−1601